Science Advances
AAAS

advances.sciencemag.org/cgi/content/full/6/26/eaba3239/DC1

Supplementary Materials for

Astrocytes and microglia play orchestrated roles and respect phagocytic territories during neuronal corpse removal in vivo

Eyiyemisi C. Damisah, Robert A. Hill, Anupama Rai, Fuyi Chen, Carla V. Rothlin, Sourav Ghosh, Jaime Grutzendler*

*Corresponding author. Email: jaime.grutzendler@yale.edu

Published 26 June 2020, *Sci. Adv.* **6**, eaba3239 (2020)
DOI: 10.1126/sciadv.aba3239

The PDF file includes:

Other Supplementary Material for this manuscript includes the following:

(available at advances.sciencemag.org/cgi/content/full/6/26/eaba3239/DC1)

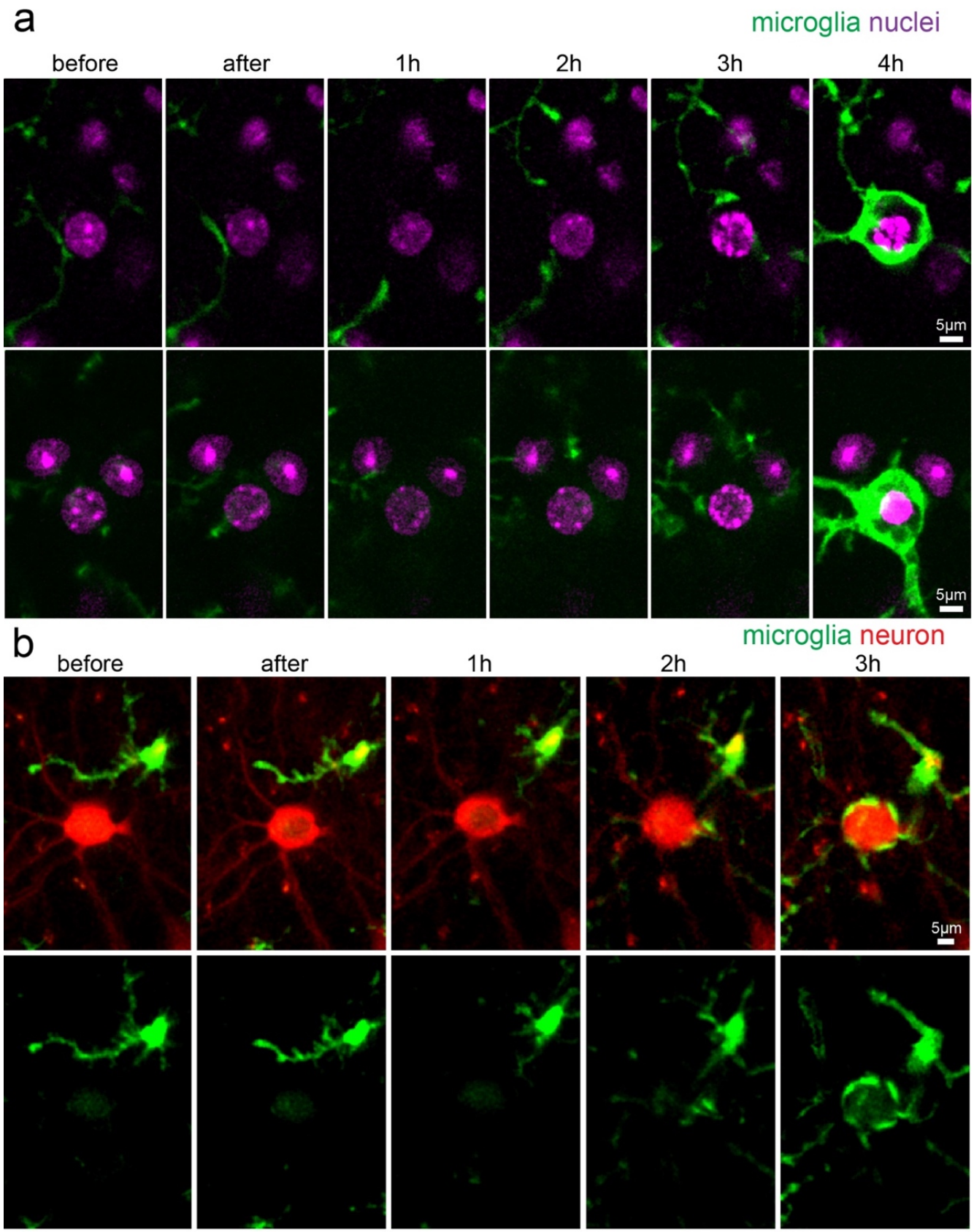

Figure S1: 2-Phatal does not induce thermal injury or immediate glial response. (**a**) *In vivo* time lapse images of Hoechst labeled nuclei (magenta) in *Cx3cr1*-GFP microglia reporter mouse showing engulfment of a single condensed nuclei (dying cell), 4 hours after 2-Phatal photochemical ablation. The microglia response is specific to only the cell with condensed nuclei and proceeds over hours. (**b**) Example of microglia (green) engulfment of a neuron (red) 3 hours after cell ablation. There is no cell rupture (top row) or microglia response (bottom row) immediately after 2Phatal photobleaching.

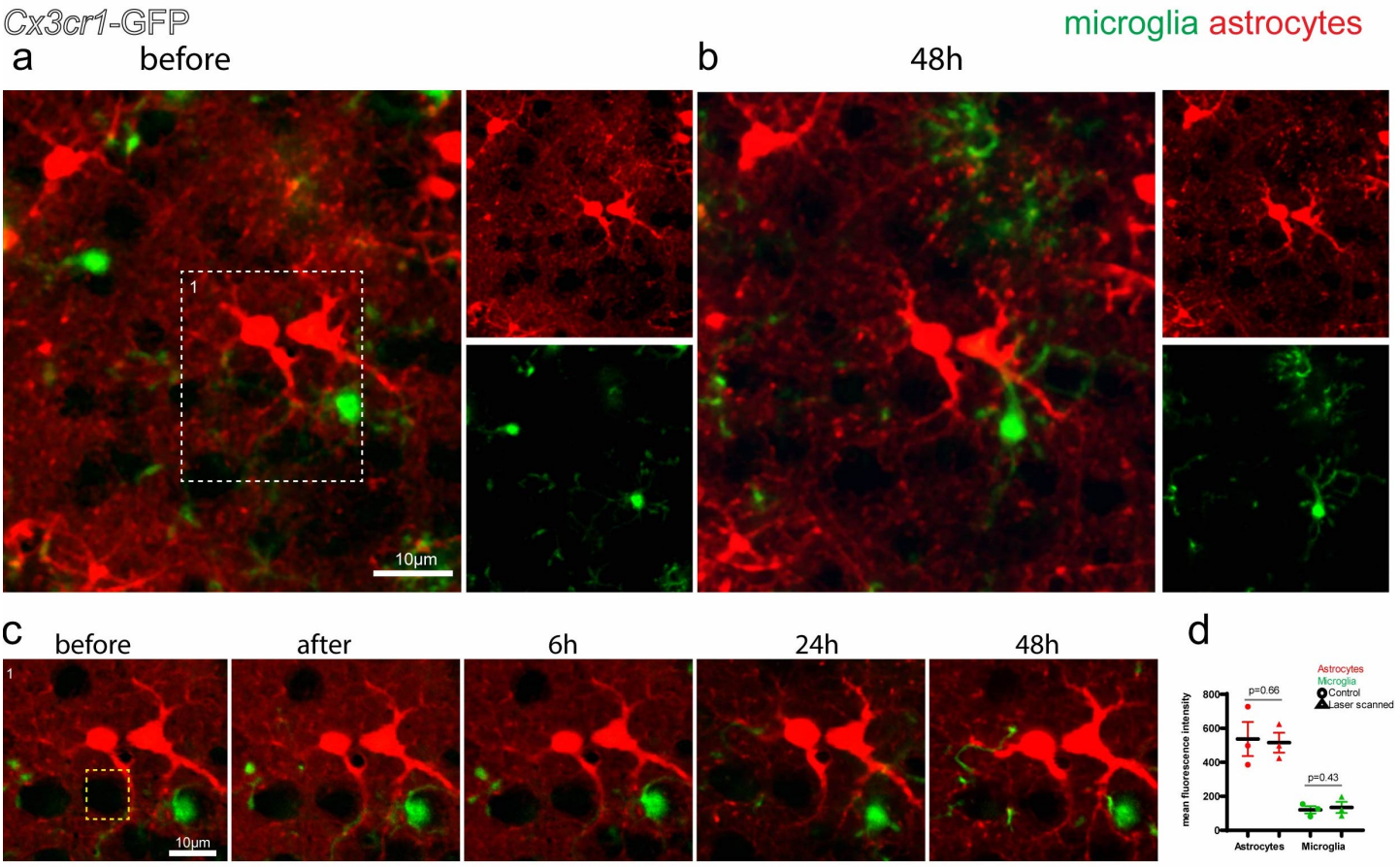

Figure S2: The laser scanning parameters used for 2-Phatal ablation do not induce glial responses in the absence of nuclear dye (**a**) *In vivo* time lapse images of astrocytes (red) labeled via SR101 in a *Cx3cr1*-GFP microglia reporter mouse before, and (**b**) 48 hours after laser scanning for 10 seconds using a 40 mW Two-photon laser. (**c**) The boxed region is magnified, and time lapse imaging shows no changes in astrocyte or microglia morphology over 48 hours after laser scanning of a cell nucleus (yellow box) using the same laser power, dwell time and frequency as is used for 2-Phatal. (**d**) Quantification of astrocyte and microglia responses at 48 hours after equal laser exposure of cell bodies in the absence of nuclear dye. SR101 or GFP intensity was measured in regions of laser scanned cells compared to adjacent control cells (p=0.66 for astrocyte polarization and p=0.43 for microglia polarization, n = 3 mice per group and 10 cells per animal, paired t-test)

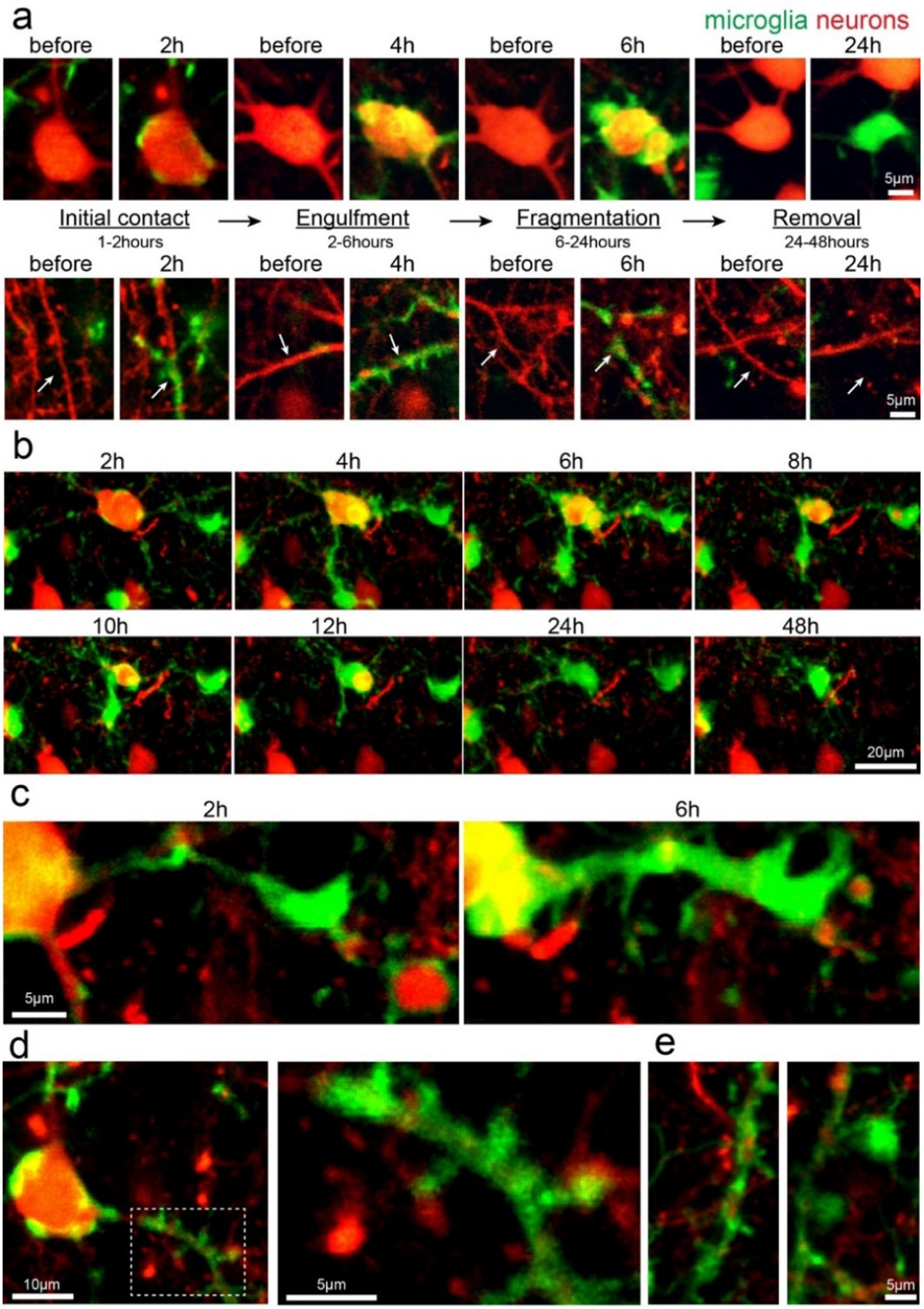

Figure S3: Stages of corpse engulfment by microglia *in vivo* (**a**) The different stages of microglia (green) engagement with a single neuron cell soma and neurites (red) after 2-Phatal. Within 4 hours, microglia contact and engulf the cell soma (top row) and neurite (bottom row). Thereafter, there is cell fragmentation within microglia and final removal in 24 hours. (**b**) Complete removal of a single neuronal soma by microglia. 2-6 hours after 2-Phatal, multiple microglia extend their processes towards the proximal dendrites and soma of the dying cell. At 6-10 hours, one microglia migrates to fully engulf the neuronal soma with retraction of other microglia processes. At 12 hours, a single microglia completely envelops and adopts the shape of the dying neuron. Fragmentation and digestion occur within 24 hours and the microglia assumes a different shape at 48 hours. (**c**) Microglial engulfment of small apoptotic neurites. (**d, e**) Microglia engulfment of proximal dendrites after 2-Phatal. The boxed region is magnified and highlights microglia engulfment of the dendritic shaft (notice the preservation of the precise dendritic spine morphology).

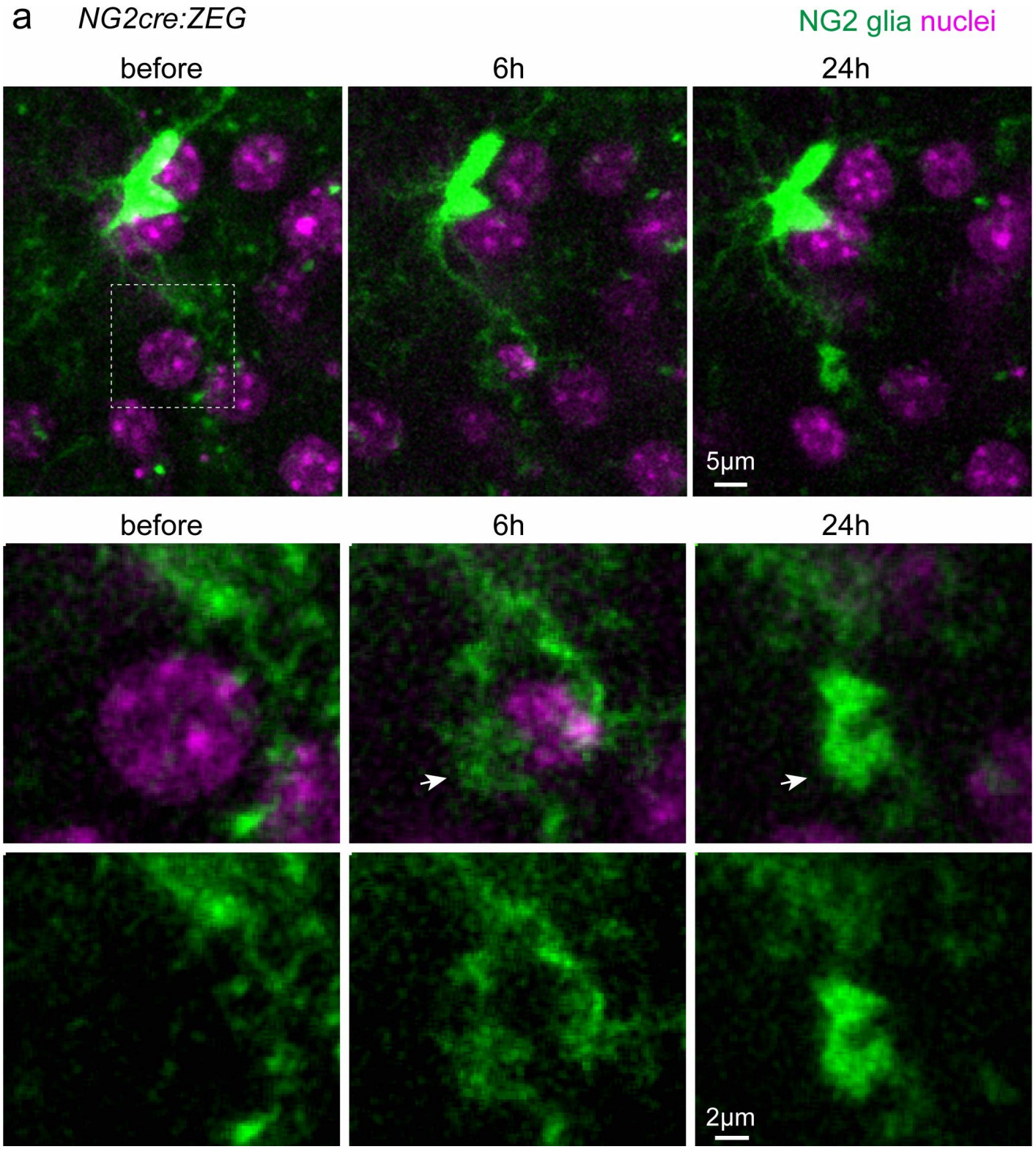

Figure S4: NG2 glia response to dying neurons after 2-Phatal *in vivo*. (**a**) An example showing the response of NG2 glia to a dying cell labeled via Hoechst dye (magenta) in NG2cre:ZEG transgenic mice. The boxed region is magnified and highlights rearrangement and polarization of NG2 glial processes towards the cell with condensed nuclei (white arrow, middle row) at 6 hours after cell ablation. Although there is complete removal of the ablated cell at 24 hours, NG2 glial processes are still polarized towards the position of the cleared cell and appear to fill the space of the removed cell.

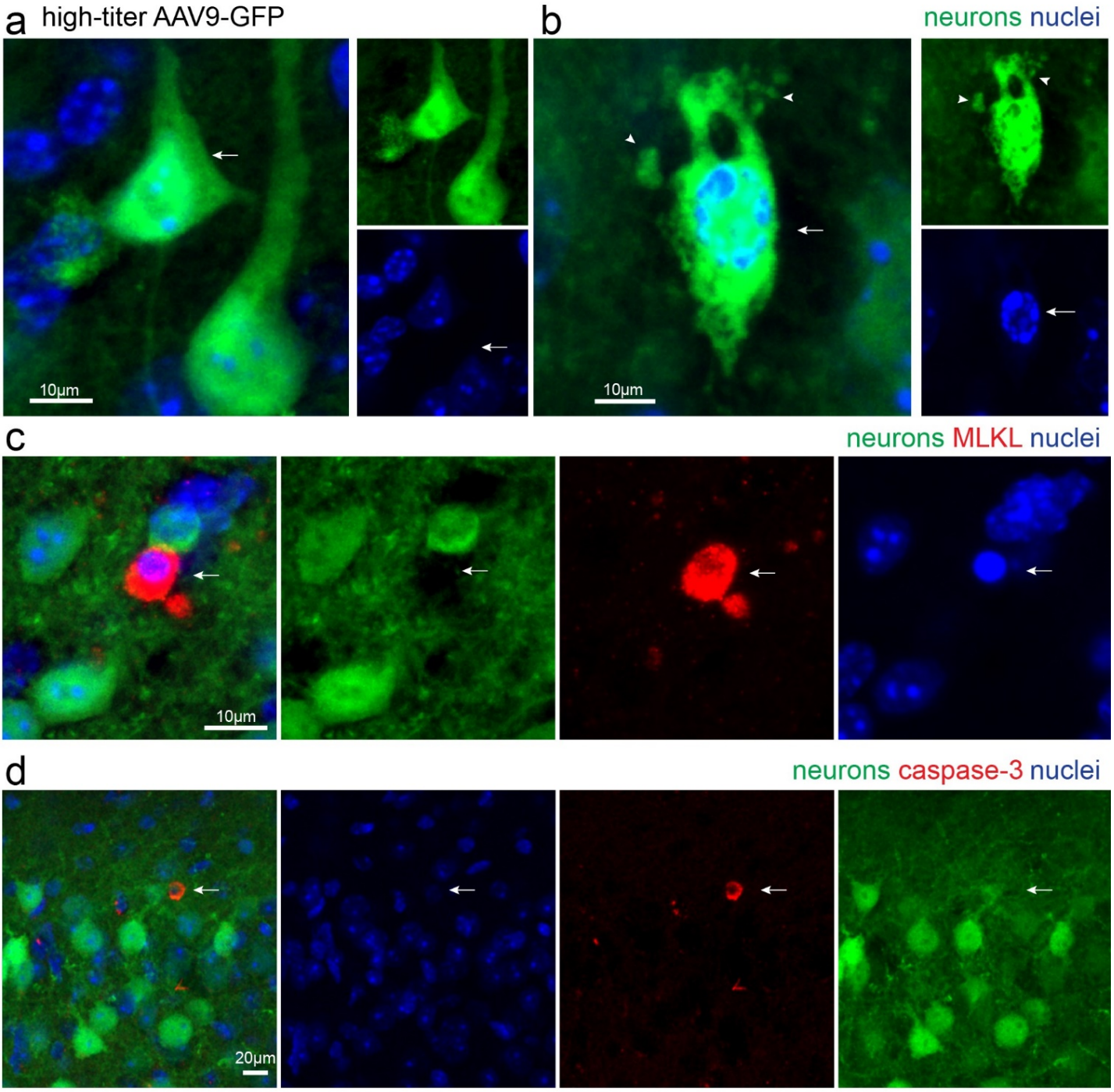

Figure S5: AAV9-induced cell death is not Caspase-3 or MLKL mediated (**a**) Image of fixed immunolabeled cortical tissue from 2-month-old mice with normal AAV9-GFP-labeled neurons (green). (**b**) Dying neurons are identified by nuclear condensation (arrow), cell fragmentation (arrowheads), and degenerative morphology. (**c**) Image of fixed immunolabeled cortical tissue from 2-month old mice showing a non-GFP labeled cell with condensed nuclei (blue) and MLKL (mixed lineage kinase domain like pseudo kinase), a marker of necroptotic cell death. (**d**) Image of fixed immunolabeled cortical tissue from 2-month old mice showing a non-GFP labeled cell with condensed nuclei (blue) and caspase 3, a marker of apoptotic cell death. None of the GFP+ dying cells were MLKL or Caspase 3 positive via immunolabeling (n = 50 GFP+ dying cells from 3 mice). Nuclei labeling via Hoechst dye (blue).

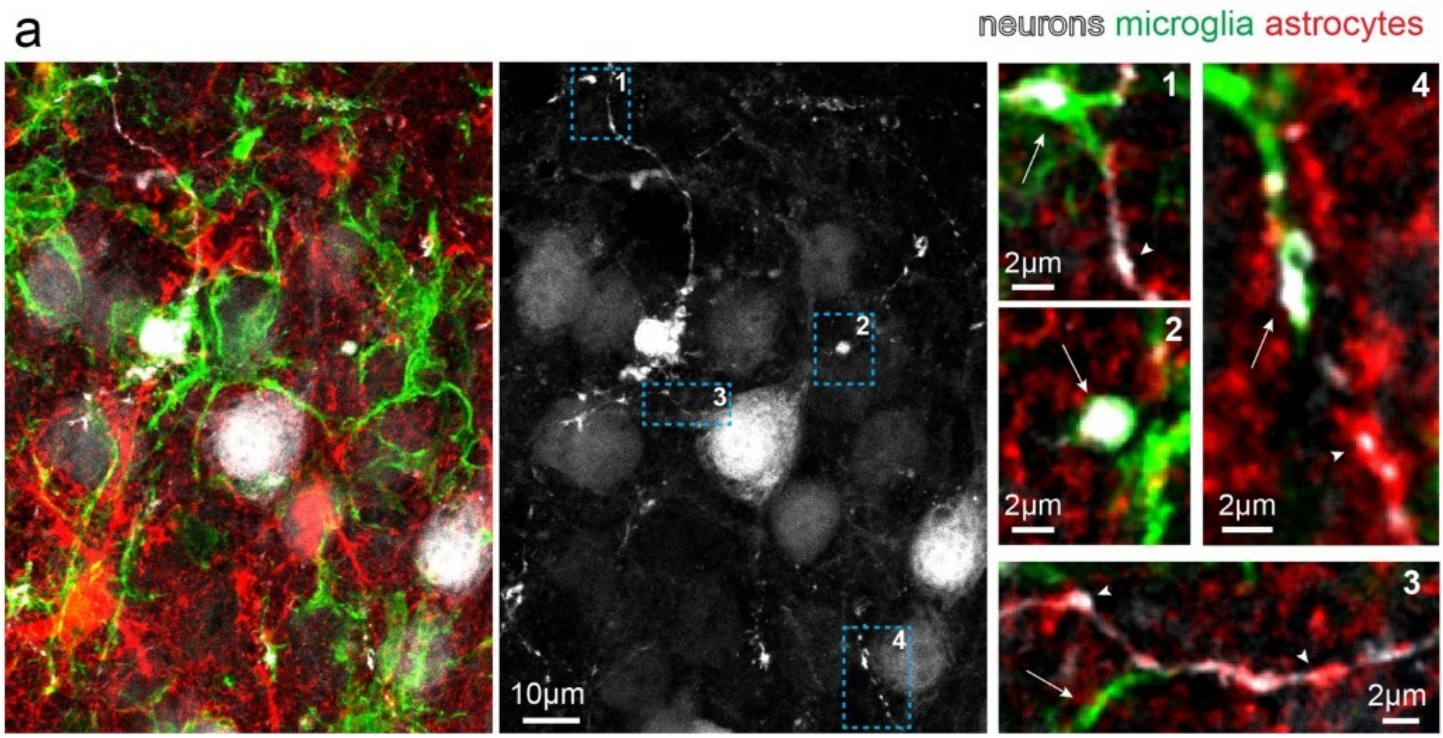

Figure S6: Astrocyte polarization and glial territorial segregation in virus mediated cell death (a) Confocal fluorescence images showing neuronal death after infection with high titer AAV9-GFP. AAV-GFP-labeled dying neurons (white) are identified by cell fragmentation and degenerating morphology. Most of the dying cells are surrounded by microglia (green) and/or astrocytes (red) exhibiting specialized roles and distinct phagocytic territories. Representative images of astrocytes (red, arrowheads) and microglia (green, arrows) contribution to the elimination of dying cells and dendrites (white) from the cortex.

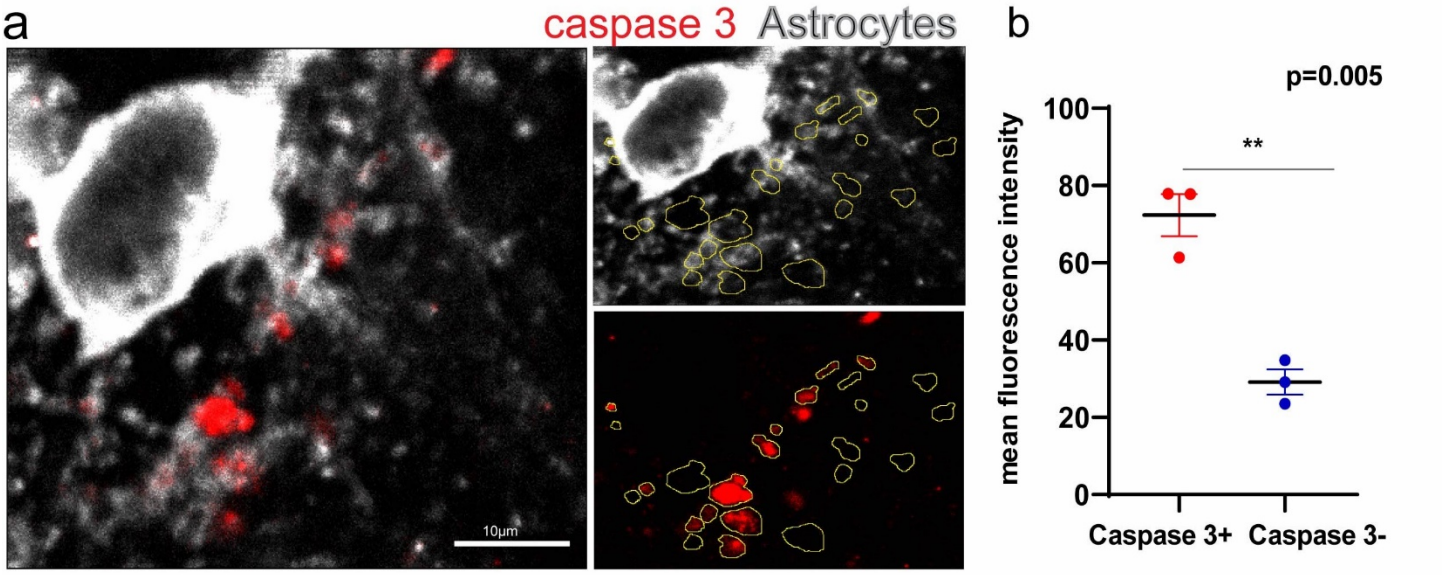

Figure S7: Astrocyte process polarization towards apoptotic neurites during spontaneous cell death in postnatal mice. (a) Confocal fluorescence image showing examples of ROI selection (brown) used for quantification of astrocyte polarization (ALDH1L1 immunolabeling, white) around caspase3 positive (red) and negative ROIs. The exact same mirror ROIs (size and shape) positioned over caspase 3 positive puncta were positioned over an immediately adjacent area of ALDH1L1 staining, as controls to compare the degree of ALDH1L1 polarization. **(b)** Quantification of mean fluorescence ALDH1L1 intensity in caspase positive versus adjacent caspase negative ROIs (p= 0.005, n=3 mice per group, greater than 30 caspase + neurites and controls per animal, paired t-test).

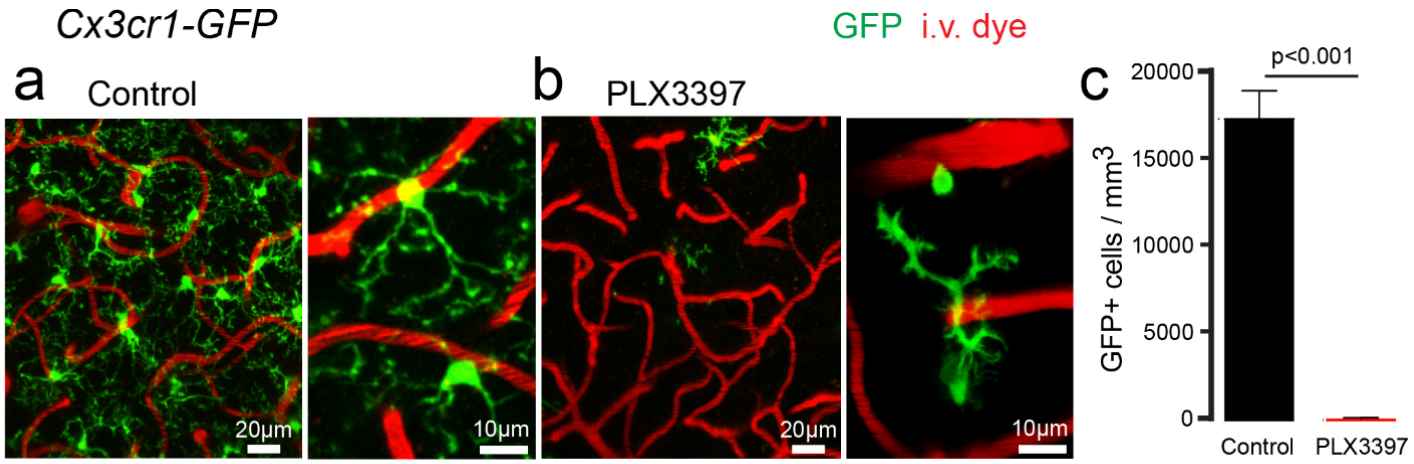

Figure S8: Pharmacological deletion of microglia following oral administration of Pexidartinib (PLX3397). (**a-b**) *In vivo* images showing the density of microglia in a *Cx3cr1*-GFP transgenic mice fed control chow or chow supplemented with PLX3397, a CSF1R inhibitor to induce elimination of microglia. (**c**) Microglia density in control compared to PLX3397 fed mice. Oral administration of PLX3397 led to over 99% elimination of brain microglia (p= <0.001, n=3 mice per group, students t-test). Cerebral vessel labeling *in vivo* was done by intravenous injection of Texas Red dextran.

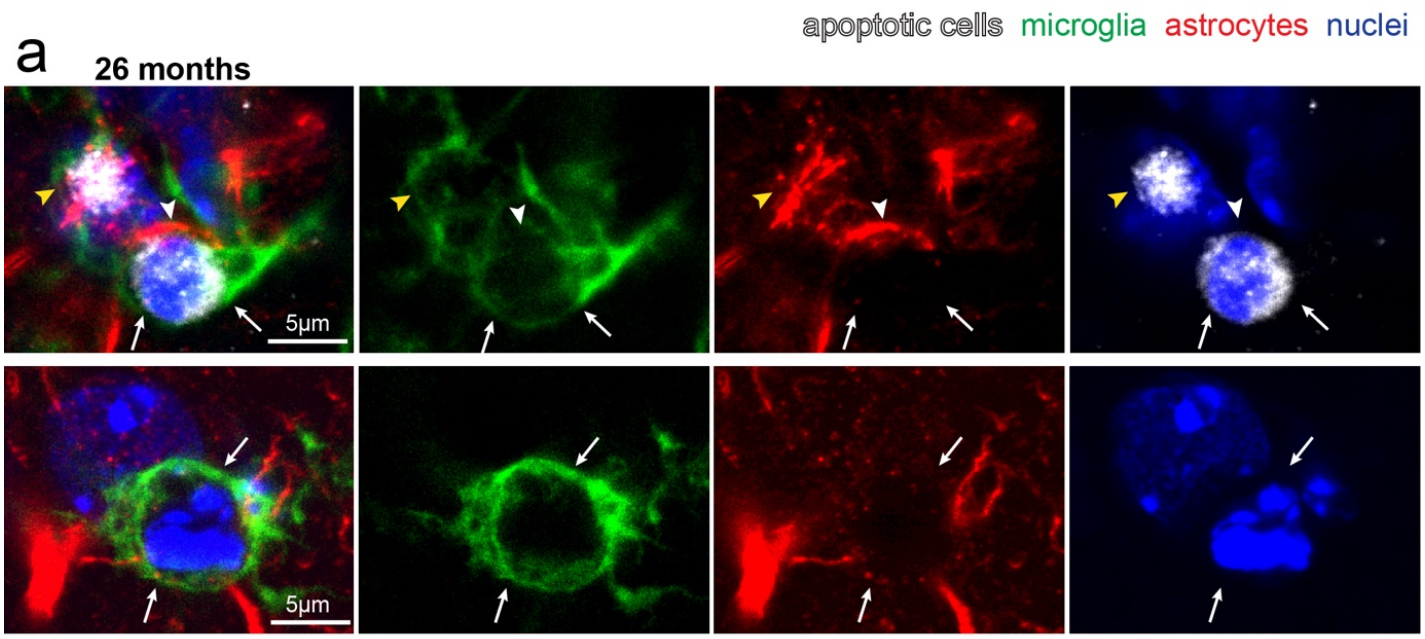

Figure S9: Apoptotic cell removal by astrocytes and microglia in the aged brain. (**a**) Image of fixed immunolabeled cortical tissue from 26-month-old mice showing a caspase 3+ apoptotic cell (white) surrounded by IBA1+ microglia (green) and ALDH1L1+ astrocytes (red). Top panel: note the precise territorial coverage of the apoptotic cell by astrocytes (white arrowhead) and microglia (yellow arrowhead and white arrows) Nuclei labeling via Hoechst dye (blue). Bottom row shows another cell with fragmented nuclei (blue) completely surrounded by microglia (green) with minimal astrocyte polarization.

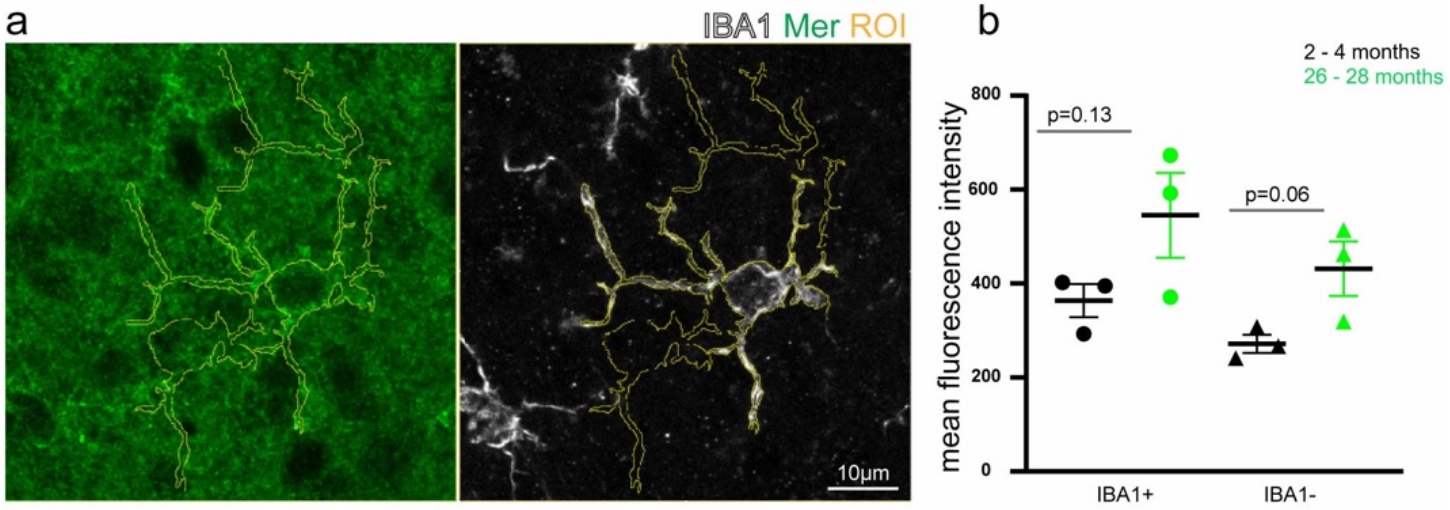

Figure S10: MER immunofluorescence quantification within microglia shows no decline in aging. **(a)** Confocal immunofluorescence image showing an example ROI selection (brown) used for quantification of MER colocalization with IBA1 (white) positive and negative regions. **(b)** Quantification of MER fluorescence mean intensity in brain sections from young and aged mice. MER intensity was measured in IBA1 positive (circle) and IBA1 negative regions (triangle). There is an overall trend towards a global increase in MER immunolabeling both within and outside microglia (p= 0.13 in IBA1 positive and p=0.06 in IBA1 negative regions, n=3 mice per group, unpaired t test).

Supplementary Movies

Movie S1: Targeted single cell photochemical apoptotic cell death
In vivo time lapse images of a neuron undergoing apoptotic cell death characterized by nuclear condensation (cyan, arrowheads), cell fragmentation, and formation of apoptotic bodies in neuronal processes (red, arrows).

Movie S2: Microglia migration and engulfment of an apoptotic neuron
Example of in vivo phagocytosis of a dying neuron (red) by microglia (green). Note microglia soma migration (arrow) and engulfment of the neuronal soma and nucleus.

Movie S3: Multiple microglia polarize towards a dying cell. Left-side video shows time lapse images of in vivo microglial dynamics after 2Phatal-induced neuronal cell death. Multiple microglia (green) polarize their processes towards the dying cell (red). Right-side video in slow-motion to show that complete engulfment of the dying cell by microglia coincides with cell swelling (arrows). Also note the protrusion of multiple microglia processes (likely from different microglia that are off the plane of view) (arrows). Some processes also appear to retract suggesting possible competition between cells for ultimate full engulfment.

Movie S4: Rapid astrocytic polarization and engulfment of small apoptotic bodies from a dying neuronal dendrite. Movie shows an example of in vivo astrocyte (magenta) engulfment of small apoptotic bodies from a disintegrating neuron (green). Astrocyte process polarization is seen around swollen and fragmented dendrites (arrows).

Movie S5: Microglia return to their baseline ramified morphology after phagocytosis. Two examples of microglia (green) engulfment of condensed and fragmented nuclei (white). Note that the thickened microglia processes during cell engulfment return to baseline. In most cases engulfment of neurons and return of microglia to their baseline phenotype occurs within 48- to 72 hours.